Supporting Information

Comparative ParaCEST effect of amide and hydroxy group in divalent Cobalt and Nickel complexes of tripyridine-based ligands

Suvam Kumar Panda,[a] Julia Torres,[b] Carlos Kremer,[b] and Akhilesh Kumar Singh*[a]

[a]Indian Institute of Technology Bhubaneswar, Khordha, Odisha, India, Pin-752050.

[b]Área de Química Inorgánica – DEC, Facultad de Química, Universidad de la República, Montevideo, 11800, Uruguay.

Contents

17. **Figure S17.** Species distribution diagram for TMTP and TDTA at 25.0 °C and I = 0.15 mol·L^{-1} $NaClO_4$.
18. **Figure S18**. Fit goodness for the protonation of TMTP (a) and TDTA (b), (0.15 M $NaClO_4$ at 25.0 °C).
19. **Figure S19.** Species distribution diagram for Co-TMTP system at 25.0 °C and I = 0.15 mol·L^{-1} $NaClO_4$. $[Co^{2+}]_{total}$ = 0.002 mol·L^{-1}, $[TMTP]_{total}$ = 0.004 mol·L^{-1}.
20. **Figure S20.** Fit goodness for the systems Co(II)-TDTA and Co(II)-TMTP (a) Ni(II)-TMTP (b), and Cu(II)-TMTP (0.15 M $NaClO_4$ at 25.0 °C).
21. **Figure S21.** ^{1}H NMR spectra of the four complexes recorded in DMSO-d_6 and upon addition of 30 µL D_2O to the same NMR tube. The exchangeable (NH) protons are represented by an * mark.
22. **Figure S22.** ^{1}H NMR spectra of the $[Co(TDTA)]^{2+}$ and $[Ni(TDTA)]^{2+}$ by varying temperature (top) and pH (bottom). Temperature variation experiments were recorded in D_2O. pH variation experiments were performed by taking 10 mM complex, 20 mM HEPES, and 100 mM NaCl at 37 °C in distilled water, a D_2O sealed capillary tube was used inside the NMR tube for locking purposes.
23. **Figure S23.** ^{1}H NMR spectra of the $[Co(TMTP)]^{2+}$ and $[Ni(TMTP)]^{2+}$ by varying temperature (top) and pH (bottom). Temperature variation experiments were recorded in D_2O. pH variation experiments were performed by taking 10 mM complex, 20 mM HEPES, and 100 mM NaCl at 37 °C in distilled water, a D_2O sealed capillary tube was used inside the NMR tube for locking purposes.
24. **Figure S24.** ^{1}H NMR spectra (400 MHz) of 10 mM of $[Co(TMTP)]^{2+}$ in aqueous solutions containing 20 mM HEPES and 100 mM NaCl, buffered at various pH values from 2 – 5. The highlighted dotted region depicts the complex dissociation at lower pH values.
25. **Figure S25.** ^{1}H NMR spectra (400 MHz) of 10 mM of $[Ni(TMTP)]^{2+}$ in aqueous solutions containing 20 mM HEPES and 100 mM NaCl, buffered at various pH values from 2 – 5. The highlighted dotted region depicts the complex dissociation at lower pH values.
26. **Figure S26.** 400 MHz NMR spectrum of the TMTP-Co complex in DMSO-d_6 with the integration of all individual peaks (* mark indicates the presence of exchangeable protons).
27. **Figure S27.** 400 MHz NMR spectrum of the TMTP-Co complex in D_2O with the identification of all paramagnetic protons and their corresponding isomers.
28. **Figure S28.** Possible isomers of the TMTP-Co complex in its solution state.

29. **Figure S29.** CEST peak positions of the amide protons in TMTP-Co and TMTP-Ni complexes.
30. **Figure S30.** CEST spectra of 10 mM $[Co(TDTA)]^{2+}$ and $[Ni(TDTA)]^{2+}$ (20 mM HEPES, pH 7.4, 400 MHz) at 37 ºC with a saturation time of 4 s and saturation power of B_1 = 25 µT
31. **Figure S31.** CEST spectra of the exchangeable proton region of 10 mM $[Co(TMTP)]^{2+}$ (left) and $[Ni(TMTP)]^{2+}$ (right) in 20 mM HEPES and 100 mM NaCl at pH 7.4 with varied pre-saturation power levels. RF pre-saturation pulse was applied for 4 s with varying saturation power of 5 µT to 25 µT for $[Co(TMTP)]^{2+}$ and 15 to 25 µT for $[Ni(TMTP)]^{2+}$.
32. **Figure S32.** Solution magnetic susceptibility data for $[Co(TDTA)]^{2+}$ (left) and $[Ni(TDTA)]^{2+}$ (right) were recorded at different pH by using 3 – 5 mM complex, 20 mM HEPES, and 100 mM NaCl at 37 °C.
33. **Figure S33.** Solution magnetic susceptibility data for $[Co(TMTP)]^{2+}$ (left) and $[Ni(TMTP)]^{2+}$ (right) were recorded at different pH by using 3 – 5 mM complex, 20 mM HEPES, and 100 mM NaCl at 37 °C.
34. **Figure S34.** UV spectrum (50 µM) of the ligand TMTP (left) and its Co(II), Ni(II), and Cu(II) complexes (right), recorded in 20 mM HEPES, and 100 mM NaCl at pH 7.4.
35. **Figure S35.** UV-Vis spectra of $[Co(TMTP)]^{2+}$ (left) and $[Ni(TMTP)]^{2+}$ (right) (5 mM) in 20 mM HEPES, and 100 mM NaCl at pH 7.4.
36. **Figure S36.** Metal displacement reaction of the $[Co(TMTP)]^{2+}$ and $[Ni(TMTP)]^{2+}$ complexes with competing Cu(II) ion, monitored for 8 hours at 264 nm. Samples containing 50 µM $[Co(TMTP)]^{2+}$ or $[Ni(TMTP)]^{2+}$ with 1, 2, and 5 equivalent ratios of $CuCl_2$ ions in aqueous solutions containing 20 mM HEPES and 100 mM NaCl buffered at pH 7.4. A 50 µM $[Co(TMTP)]^{2+}$ sample is present to determine the absorbance of a 100% dissociation.
37. **Figure S37.** UV-Vis kinetic study of the complexes $[Co(TMTP)]^{2+}$ and $[Ni(TMTP)]^{2+}$ at 264 nm in acidic conditions, pH 4, (left) and in the presence of competing anions like 25 mM K_2CO_3 and 0.4 mM K_2HPO_4 (right).
38. **Figure S38.** Cyclic voltammogram of $[Co(TMTP)]^{2+}$ (left) and $[Ni(TMTP)]^{2+}$ (right) recorded in an aqueous phase contained 1 mM complex, 20 mM HEPES, and 100 mM NaCl (pH = 7.4).
39. **Table S1.** Selected bond angles of the four complexes.

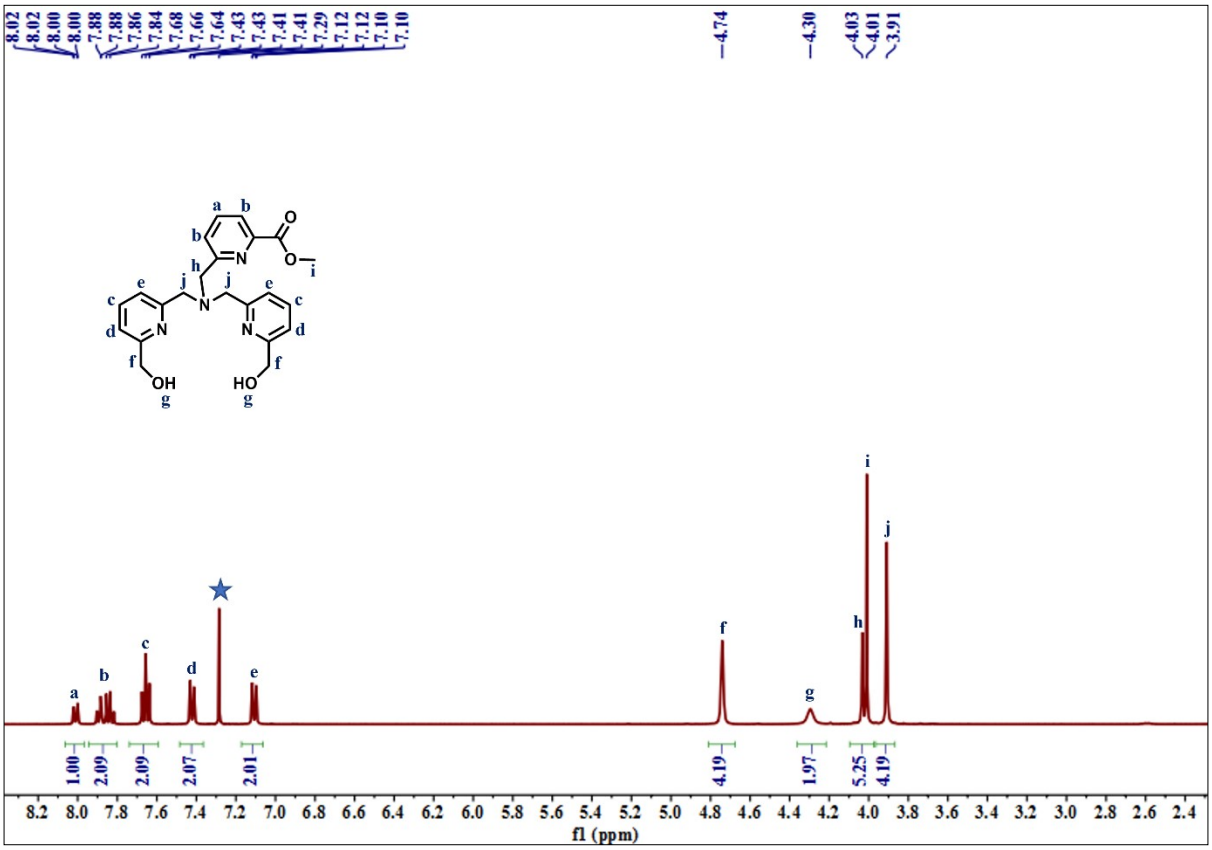

Figure S1. ^{1}H NMR (400 MHz) of compound 3 recorded in $CDCl_3$ (* mark indicates the residual peak of solvent).

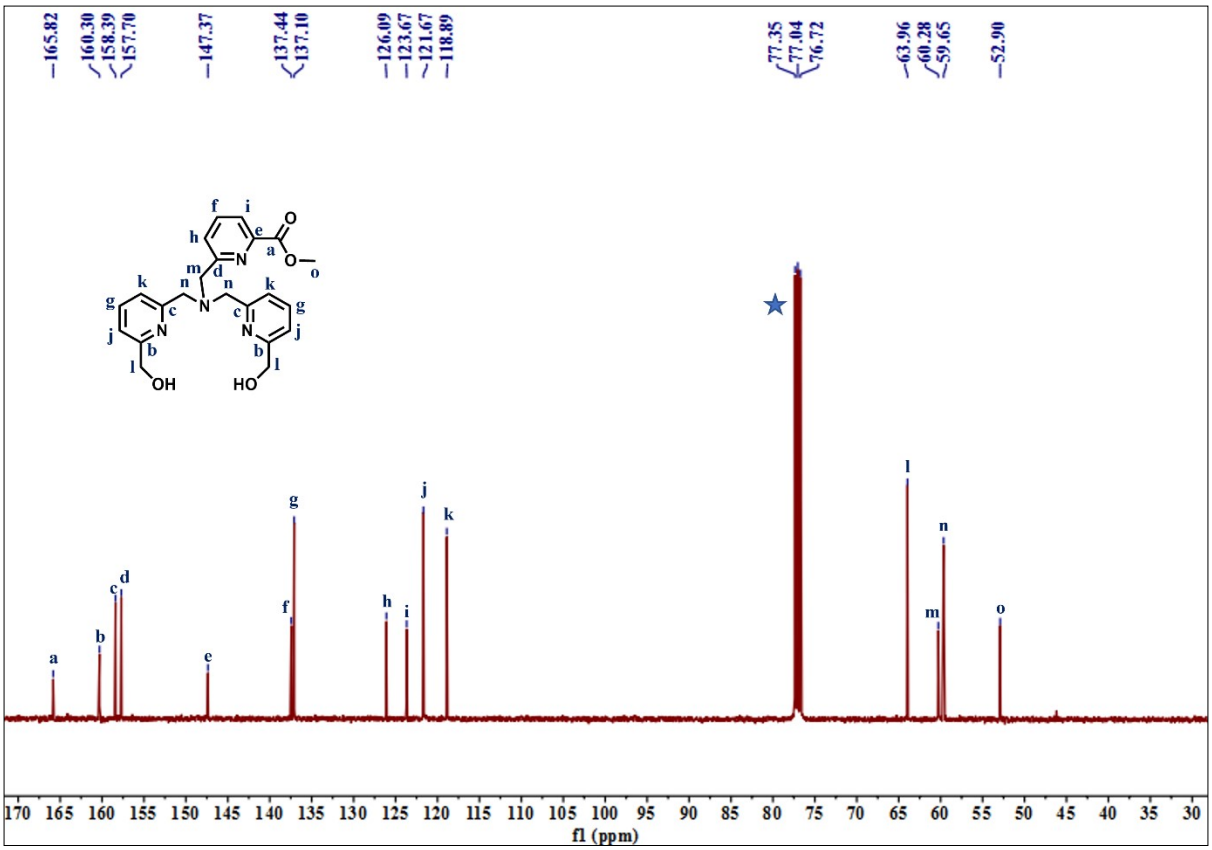

Figure S2. ^{13}C NMR (100 MHz) of compound 3 recorded in $CDCl_3$ (* mark indicates the residual peak of solvent).

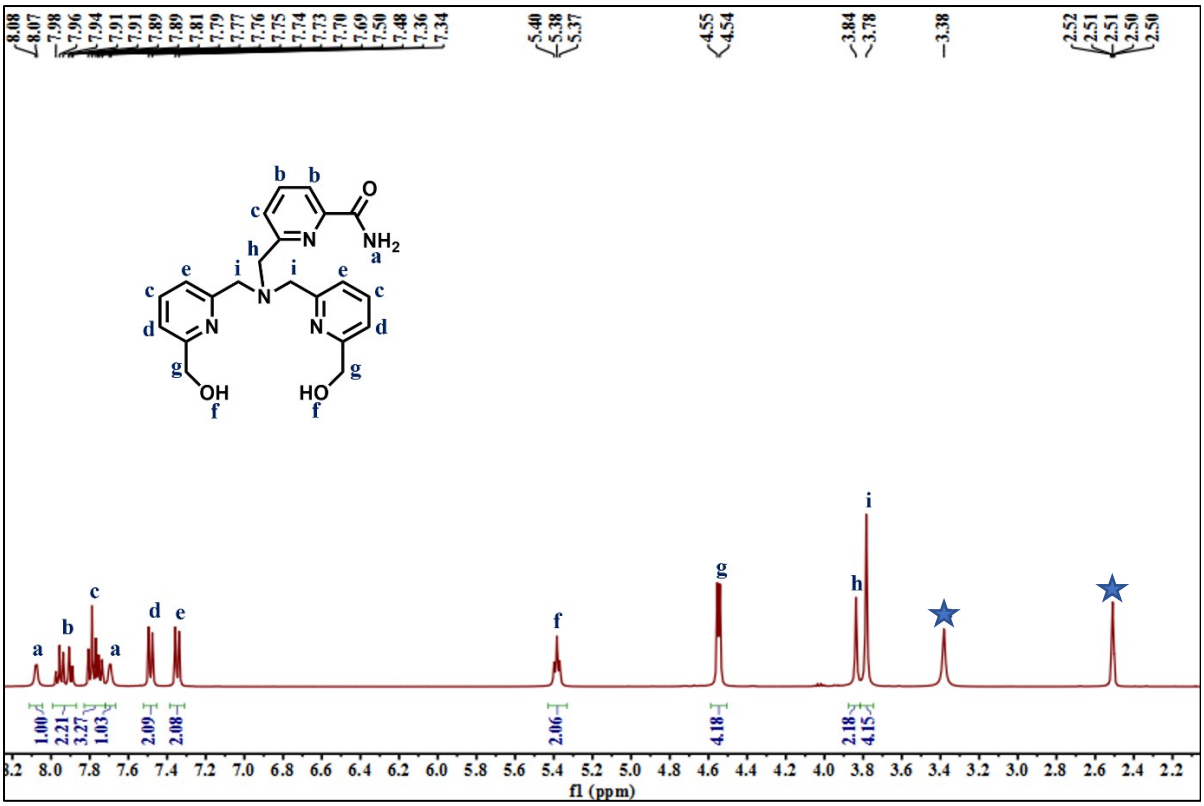

Figure S3. ^{1}H NMR (400 MHz) of TDTA recorded in DMSO-d_6 (* mark indicates the residual peak of solvent).

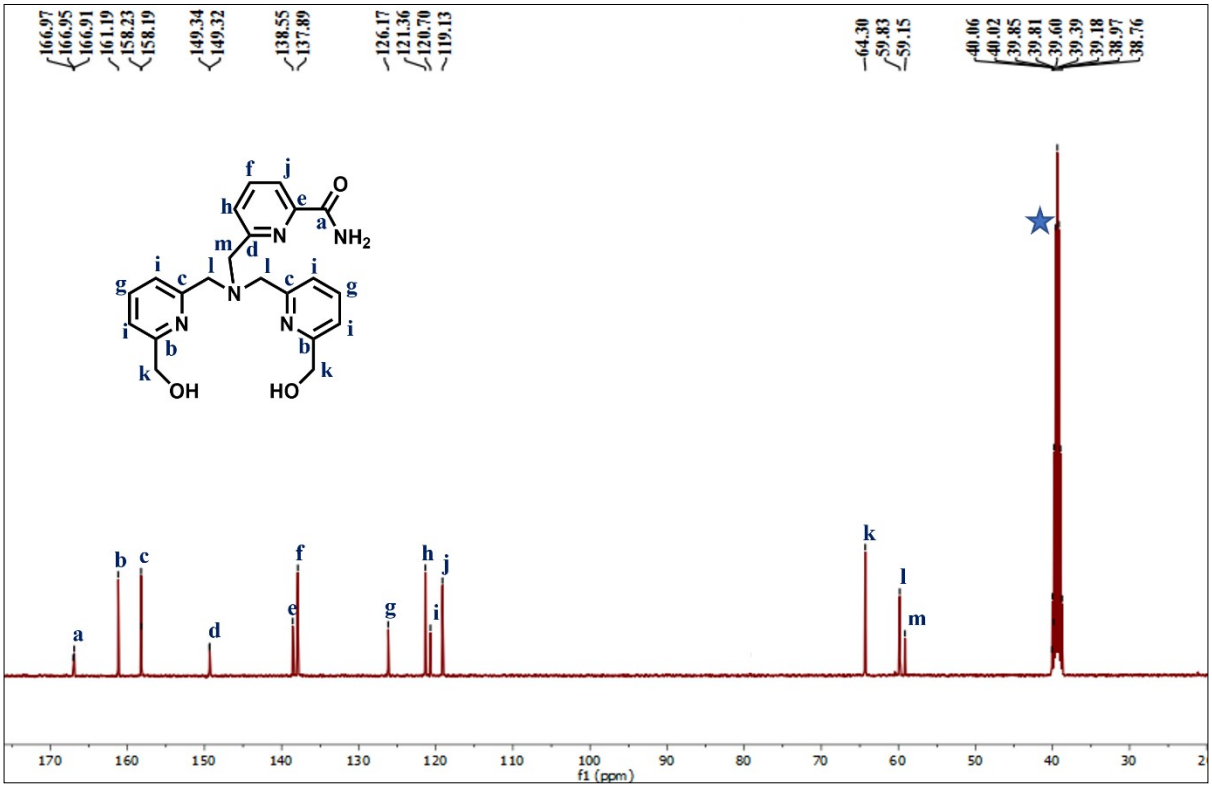

Figure S4. ^{13}C NMR (100 MHz) of TDTA recorded in DMSO-d_6 (* mark indicates the residual peak of solvent).

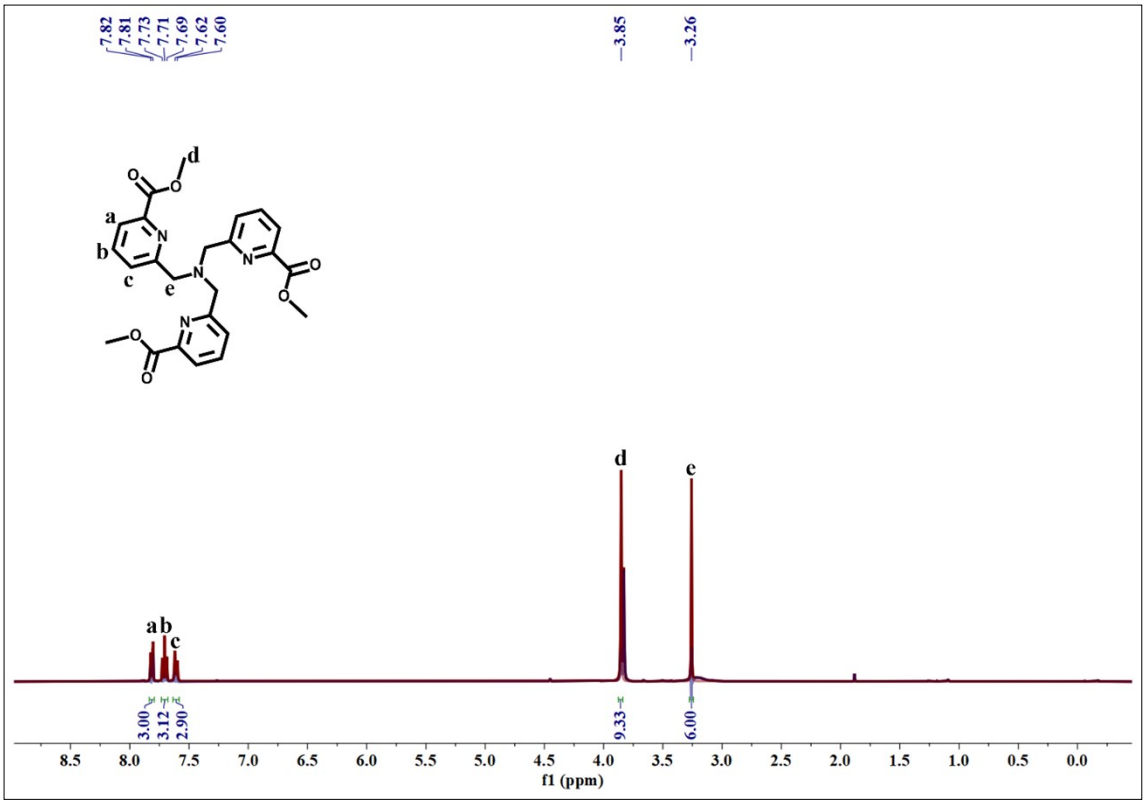

Figure S5. ^{1}H NMR (400 MHz) of compound 4 recorded in $CDCl_3$.

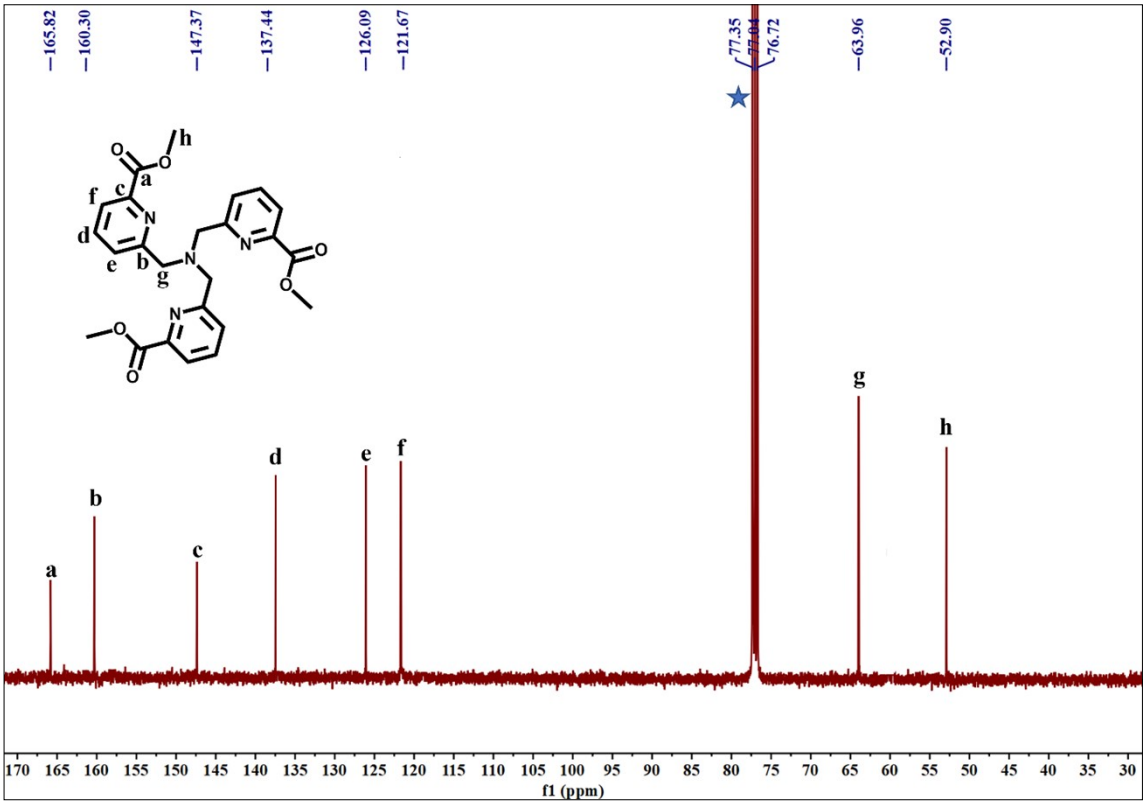

Figure S6. ^{13}C NMR (100 MHz) of compound 4 recorded in $CDCl_3$ (* mark indicates the residual peak of solvent).

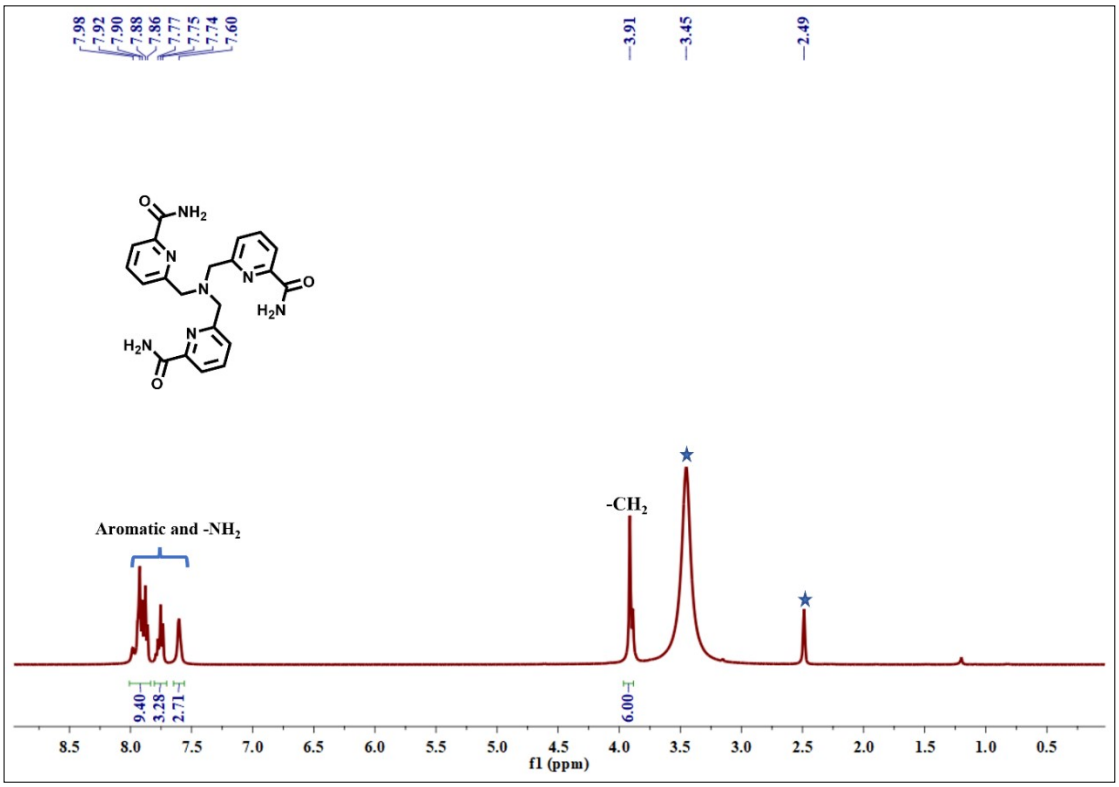

Figure S7. ^{1}H NMR (400 MHz) of TMTP recorded in DMSO-d_6 (* mark indicates the residual peak of solvent).

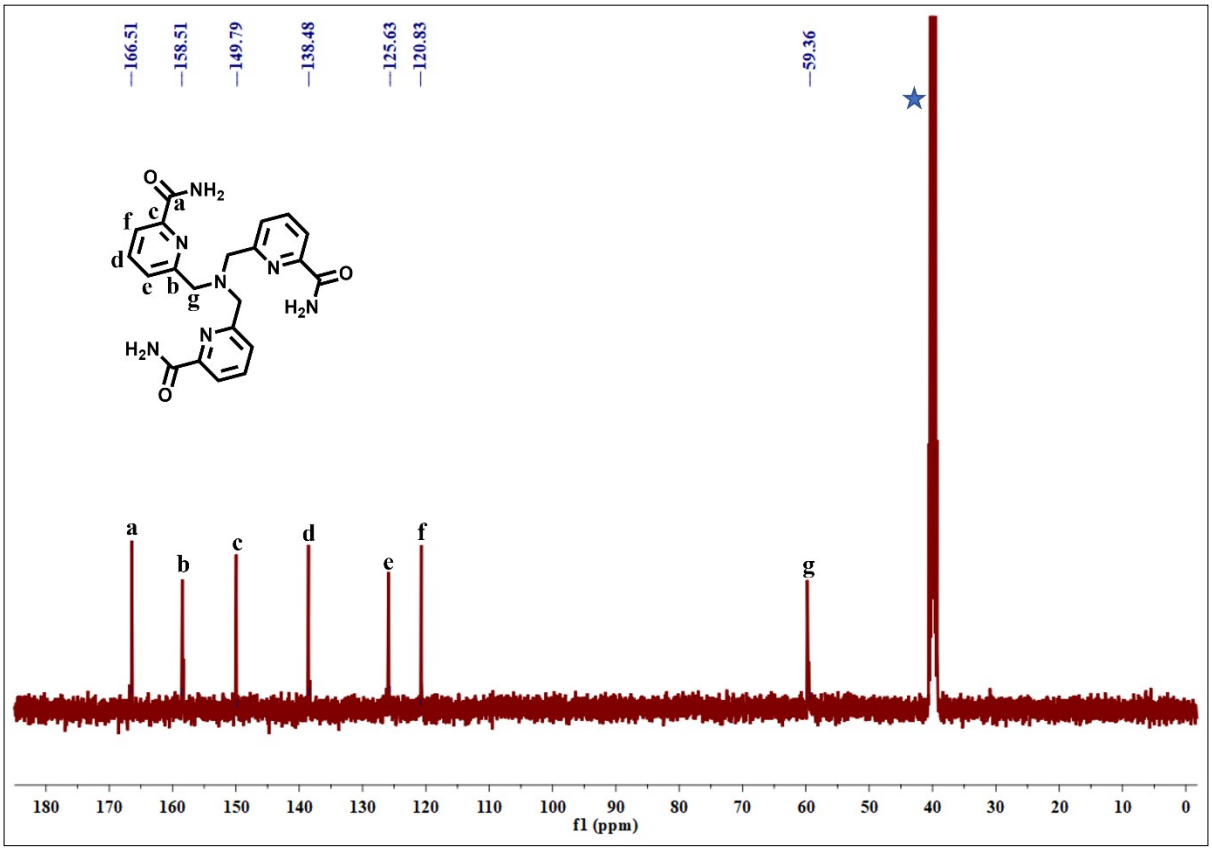

Figure S8. ^{13}C NMR (100 MHz) of TMTP recorded in DMSO-d_6 (* mark indicates the residual peak of solvent).

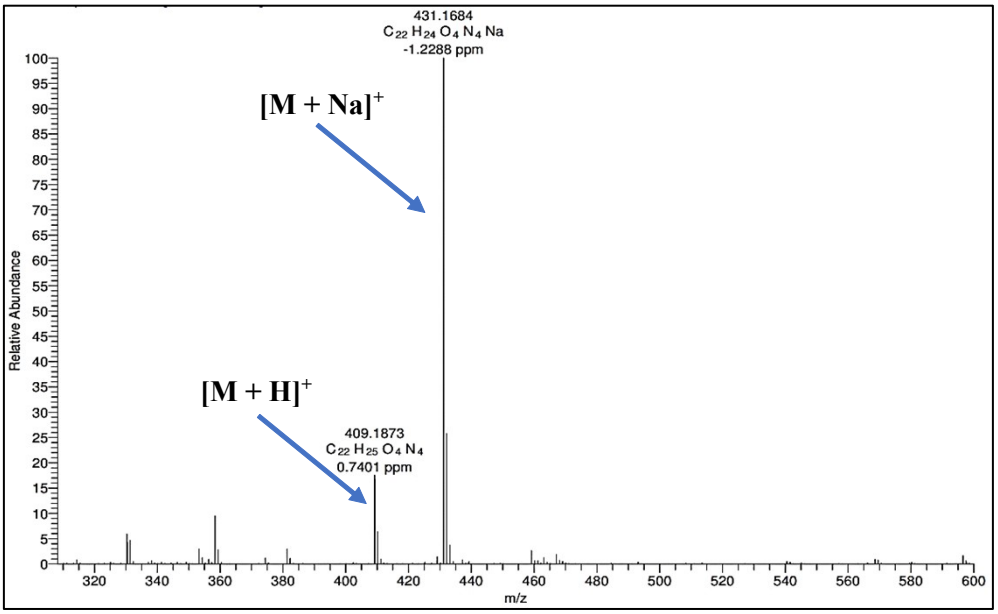

Figure S9. HRMS spectrum of compound 3.

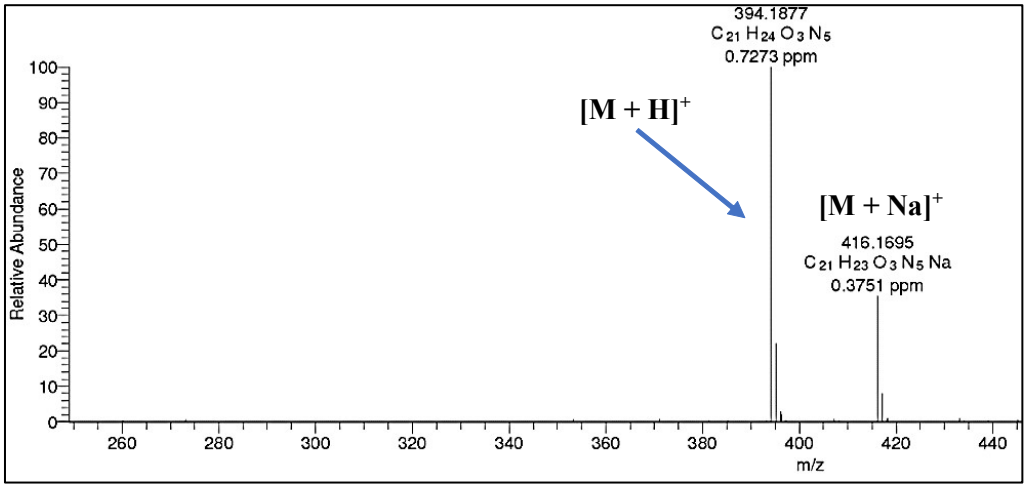

Figure S10. HRMS spectrum of ligand TDTA.

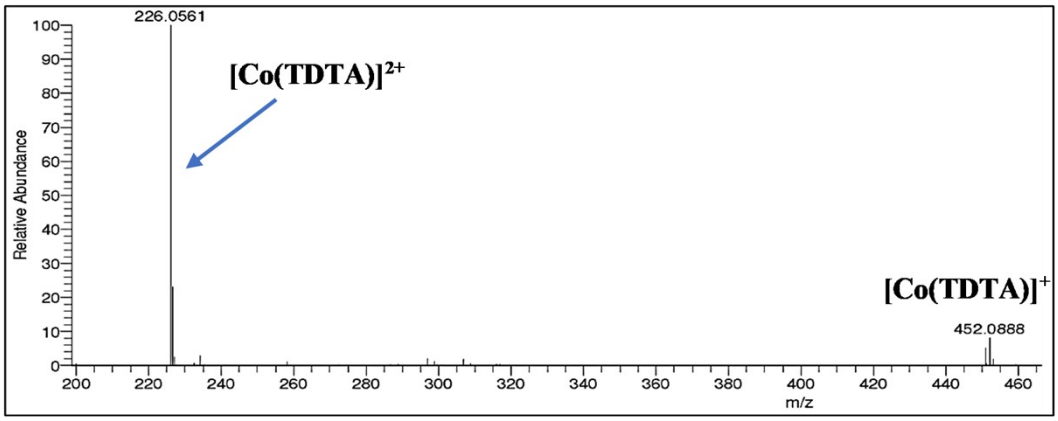

Figure S11. HRMS spectrum of $[Co(TDTA)]^{2+}$.

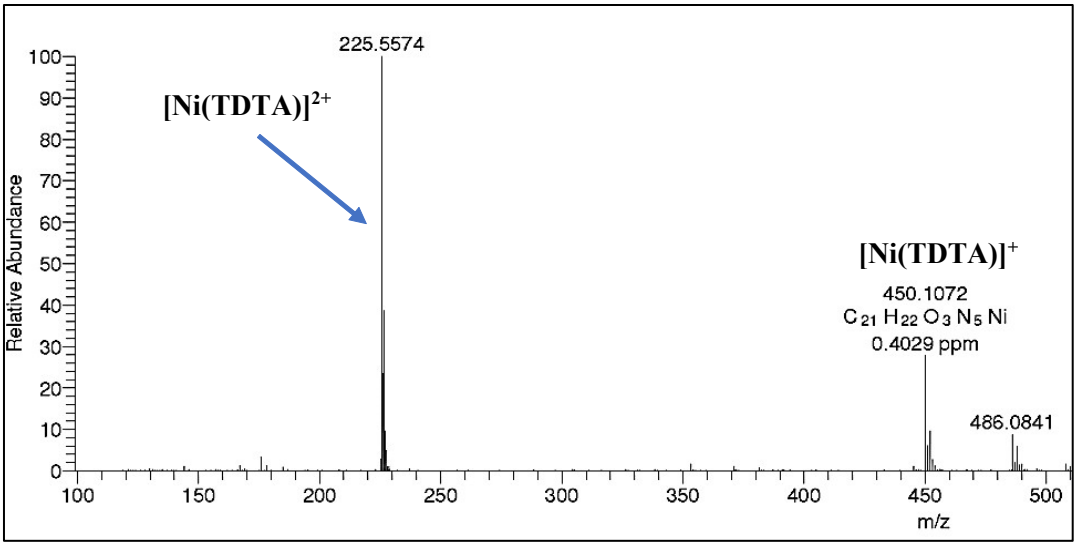

Figure S12. HRMS spectrum of $[Ni(TDTA)]^{2+}$.

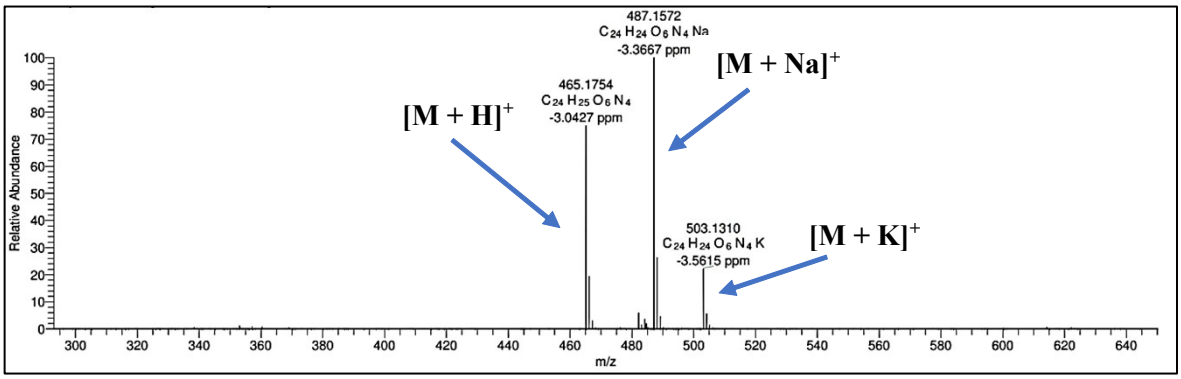

Figure S13. HRMS spectrum of compound 4.

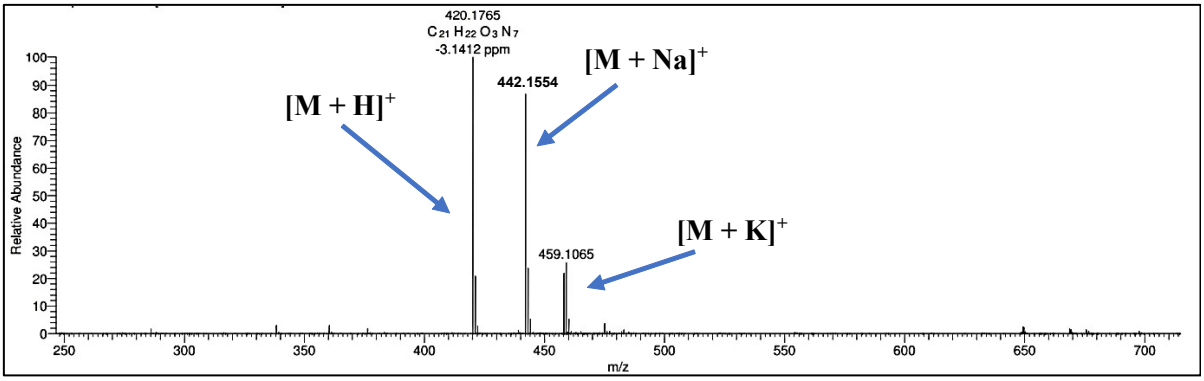

Figure S14. HRMS spectrum of ligand TMTP.

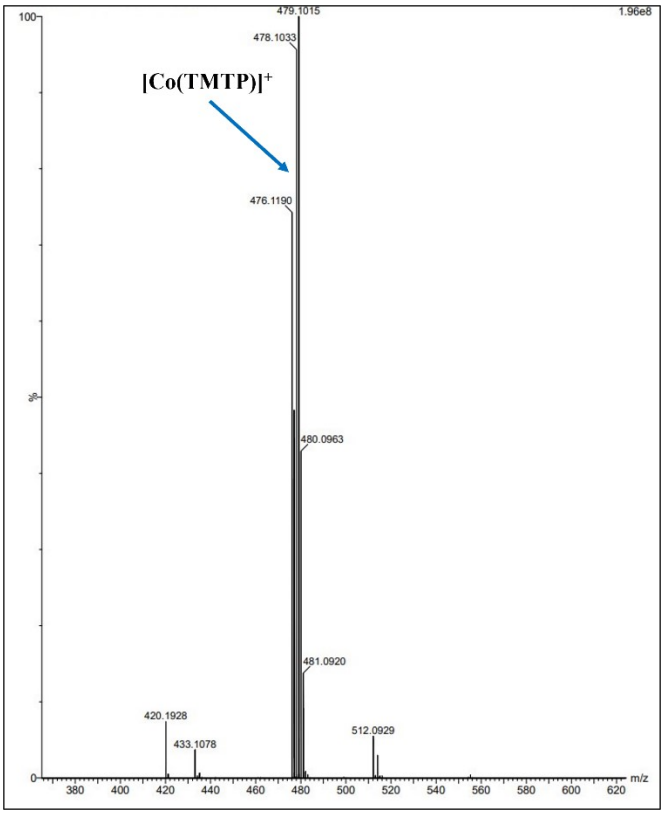

Figure S15. HRMS spectrum of $[Co(TMTP)]^+$.

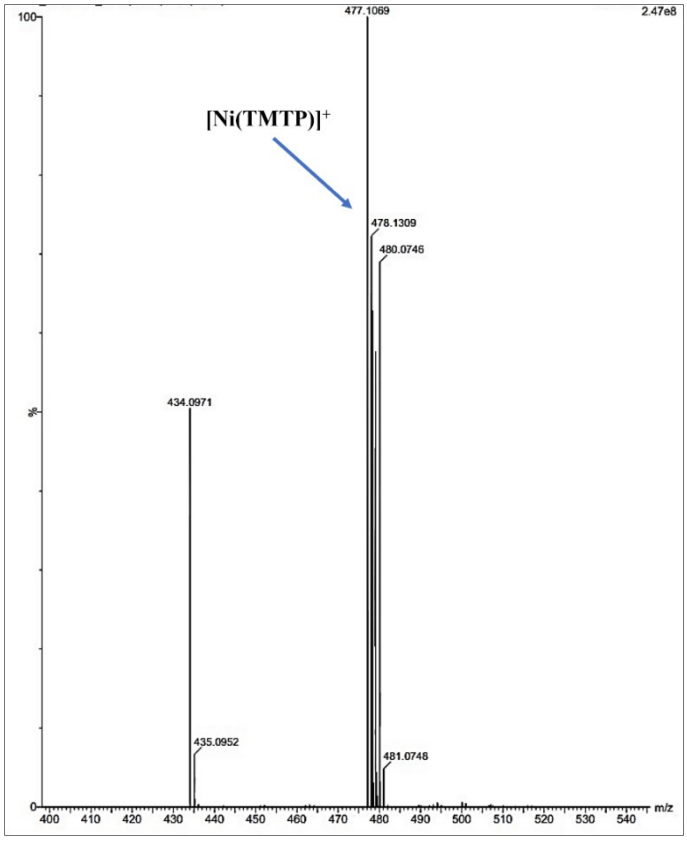

Figure S16. HRMS spectrum of $[Ni(TMTP)]^+$.

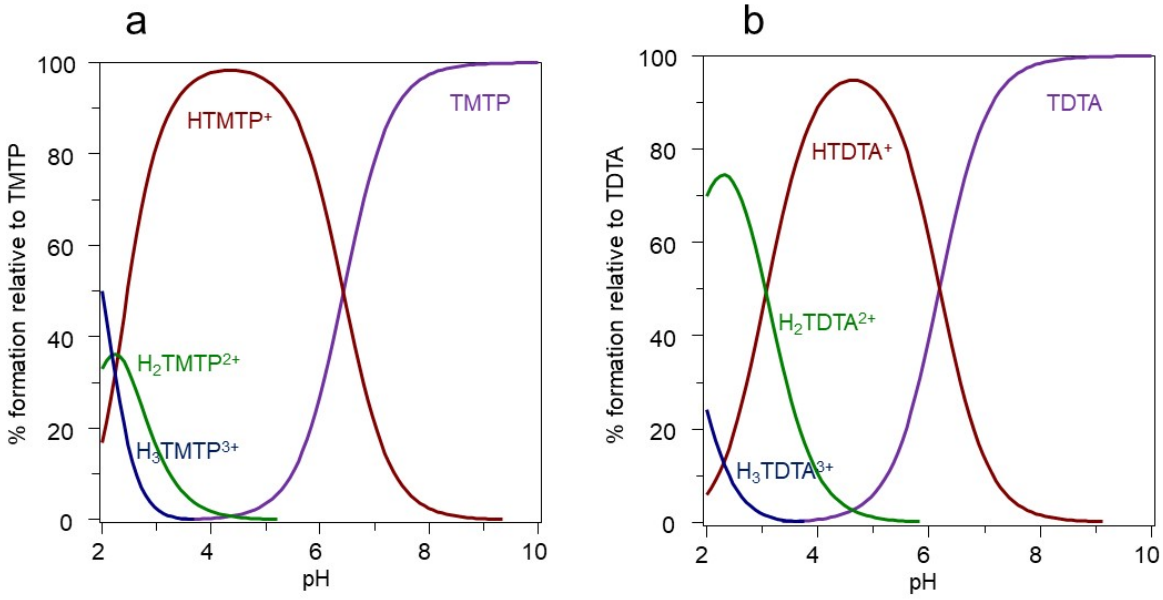

Figure S17. Species distribution diagram for TMTP and TDTA at 25.0 °C and $I = 0.15$ mol·L^{-1} $NaClO_4$.

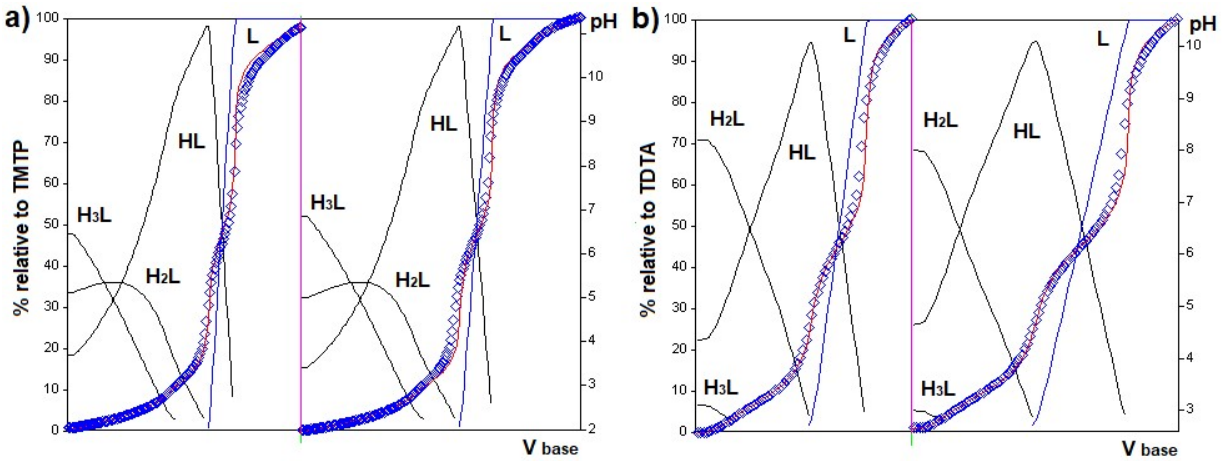

Figure S18. Fit goodness for the protonation of TMTP (a) and TDTA (b), (0.15 M $NaClO_4$ at 25.0 °C).

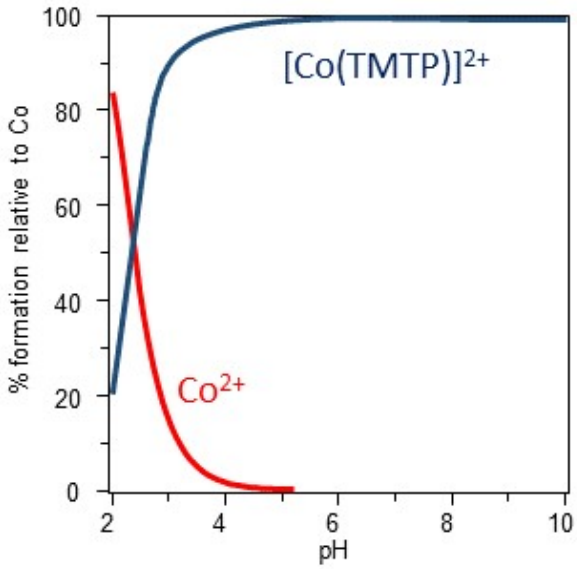

Figure S19. Species distribution diagram for Co-TMTP system at 25.0 °C and I = 0.15 mol·L^{-1} $NaClO_4$. $[Co^{2+}]_{total}$ = 0.002 mol·L^{-1}, $[TMTP]_{total}$ = 0.004 mol·L^{-1}.

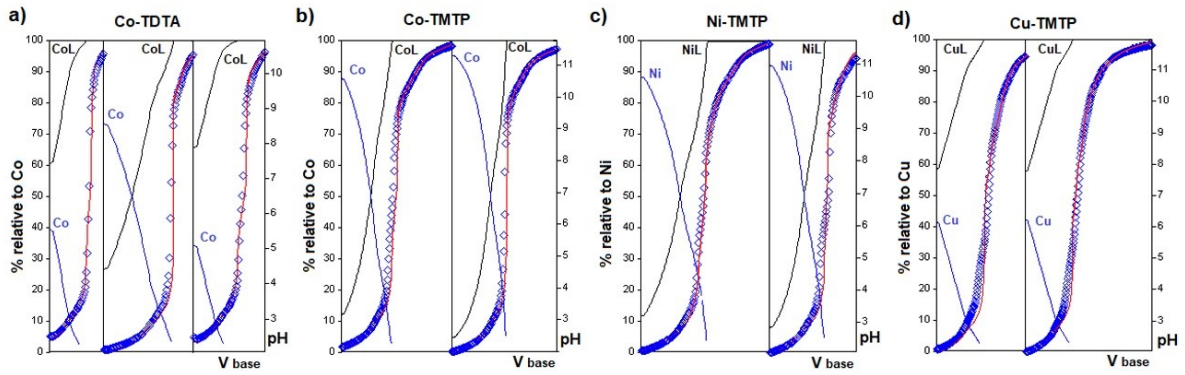

Figure S20. Fit goodness for the systems Co(II)-TDTA (a), Co(II)-TMTP (b), Ni(II)-TMTP (c), and Cu(II)-TMTP (d) (0.15 M $NaClO_4$ at 25.0 °C).

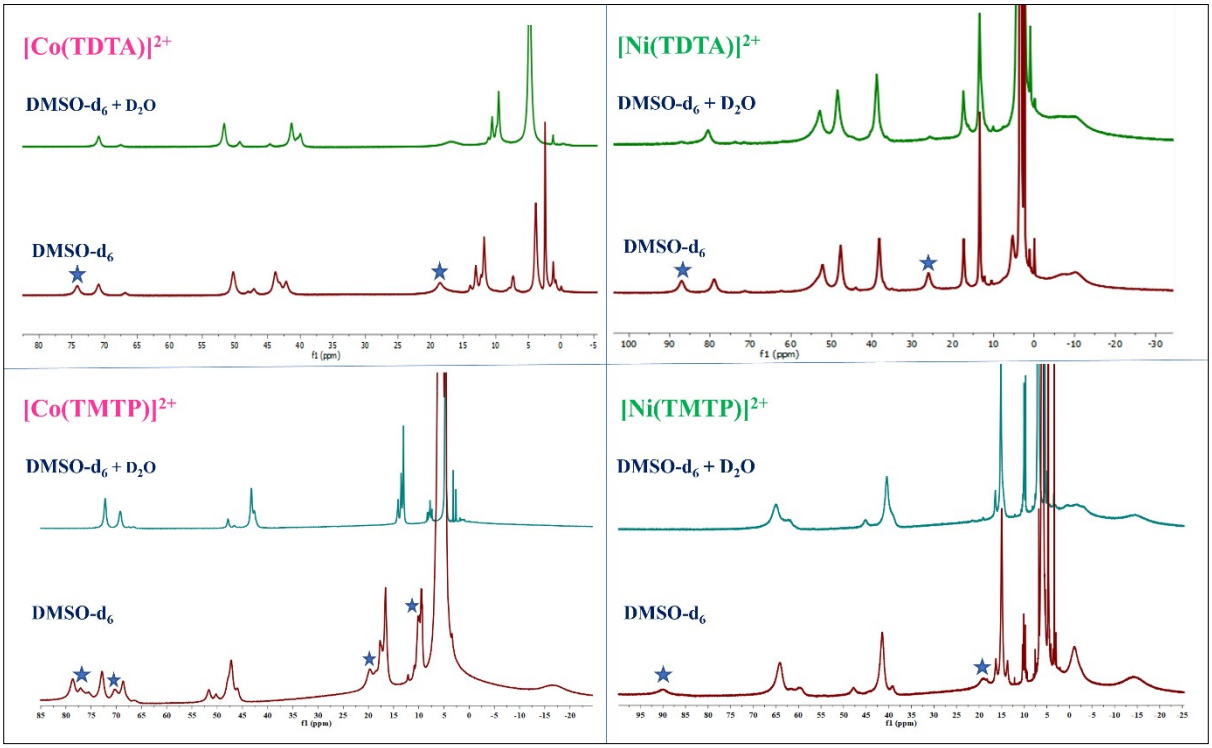

Figure S21. ^{1}H NMR spectra of the four complexes recorded in DMSO-d_6 and upon addition of 30 µL D_2O to the same NMR tube. The exchangeable protons are represented by an * mark.

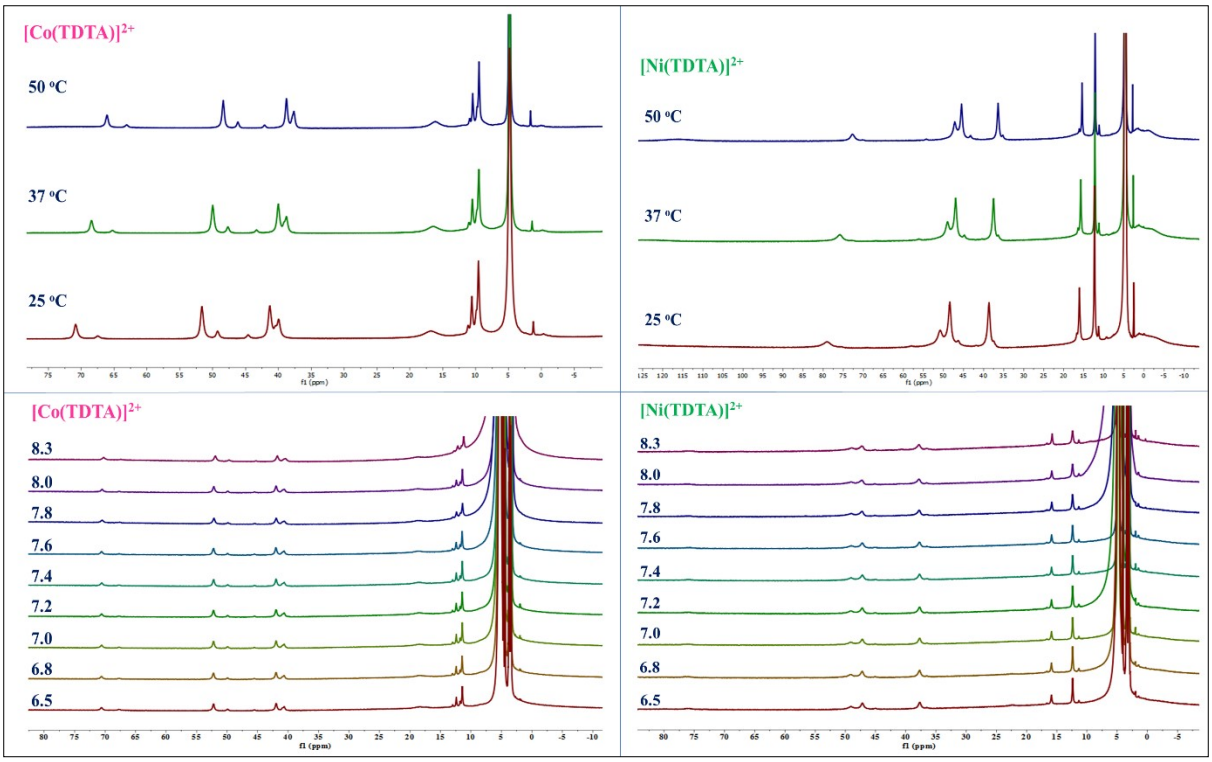

Figure S22. ^{1}H NMR spectra of the $[Co(TDTA)]^{2+}$ and $[Ni(TDTA)]^{2+}$ by varying temperature (top) and pH (bottom). Temperature variation experiments were recorded in D_2O. pH variation experiments were performed by taking 10 mM complex, 20 mM HEPES, and 100 mM NaCl at 37 °C in distilled water, a D_2O-sealed capillary tube was used inside the NMR tube for locking purposes.

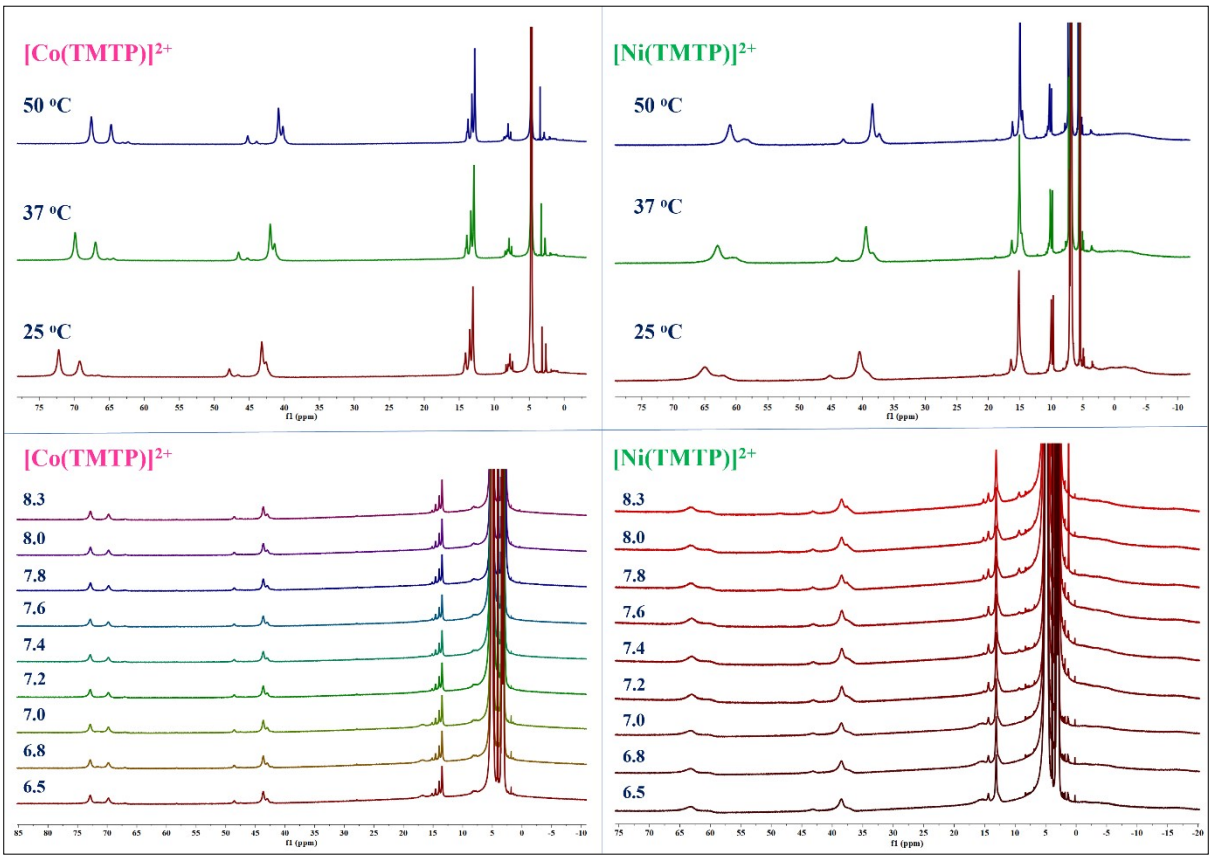

Figure S23. ^{1}H NMR spectra of the $[Co(TMTP)]^{2+}$ and $[Ni(TMTP)]^{2+}$ by varying temperature (top) and pH (bottom). Temperature variation experiments were recorded in D_2O. pH variation experiments were performed by taking 10 mM complex, 20 mM HEPES, and 100 mM NaCl at 37 °C in distilled water, a D_2O-sealed capillary tube was used inside the NMR tube for locking purposes.

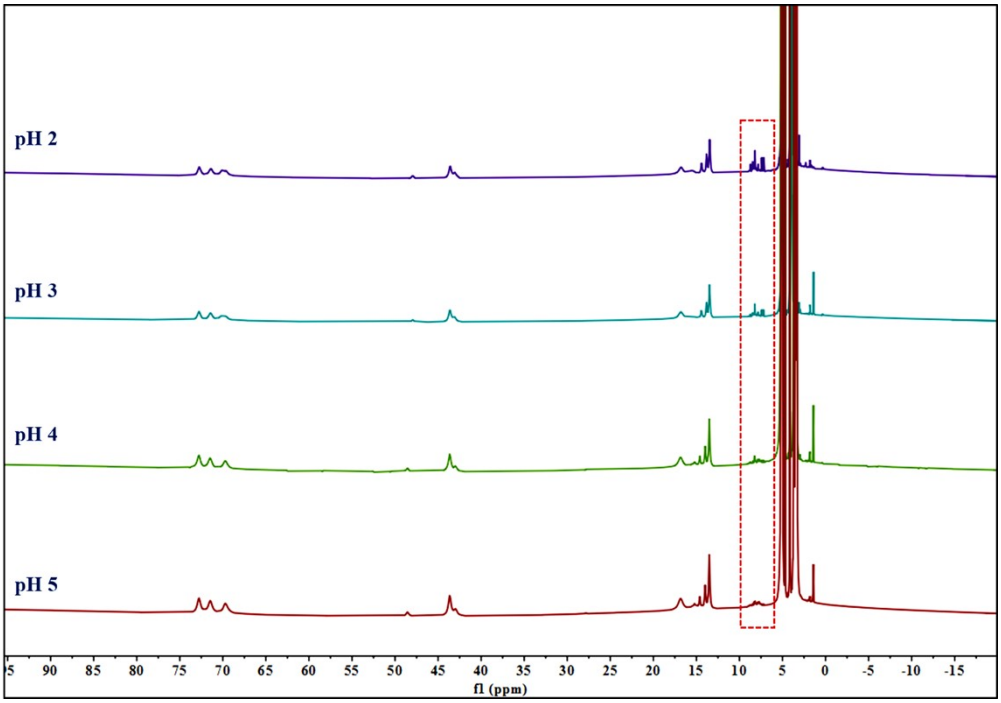

Figure S24. ^{1}H NMR spectra (400 MHz) of 10 mM of $[Co(TMTP)]^{2+}$ in aqueous solutions containing 20 mM HEPES and 100 mM NaCl, buffered at various pH values from 2 – 5. The highlighted dotted region depicts the complex dissociation at lower pH values.

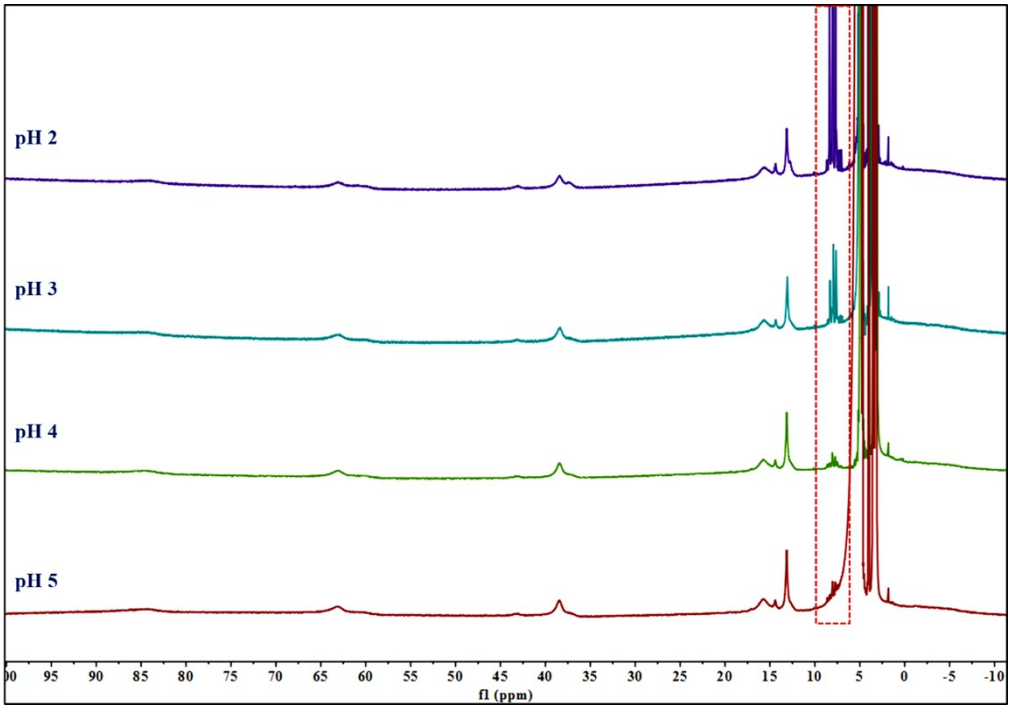

Figure S25. ^{1}H NMR spectra (400 MHz) of 10 mM of $[Ni(TMTP)]^{2+}$ in aqueous solutions containing 20 mM HEPES and 100 mM NaCl, buffered at various pH values from 2 – 5. The highlighted dotted region depicts the complex dissociation at lower pH values.

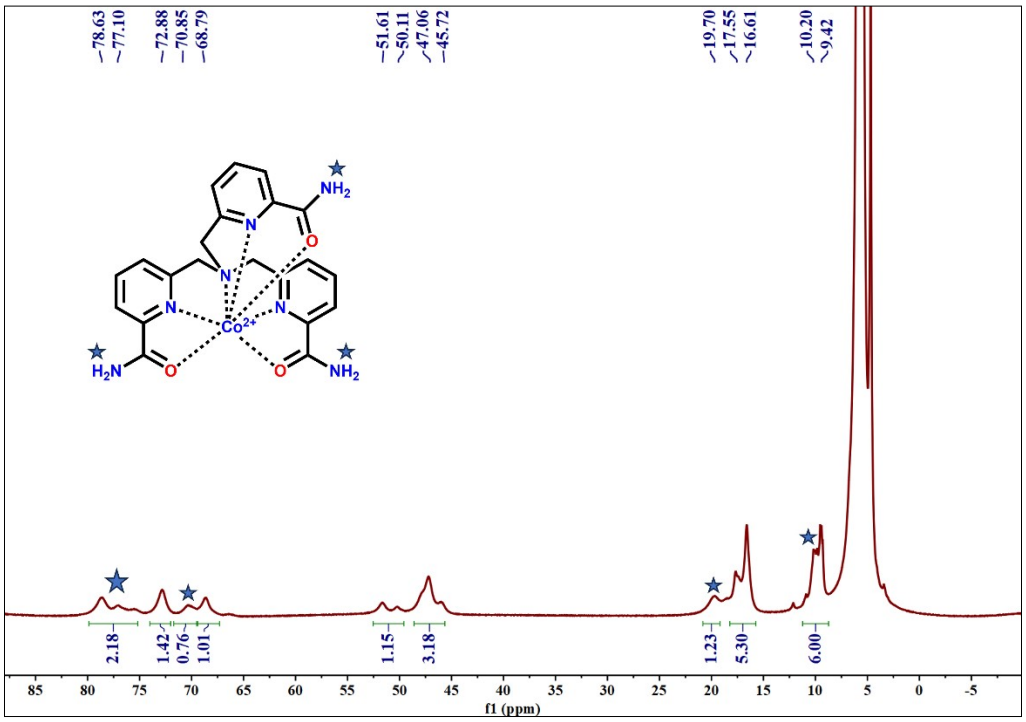

Figure S26. 400 MHz NMR spectrum of the TMTP-Co complex in DMSO-d_6 with the integration of all individual peaks (* mark indicates the presence of exchangeable protons).

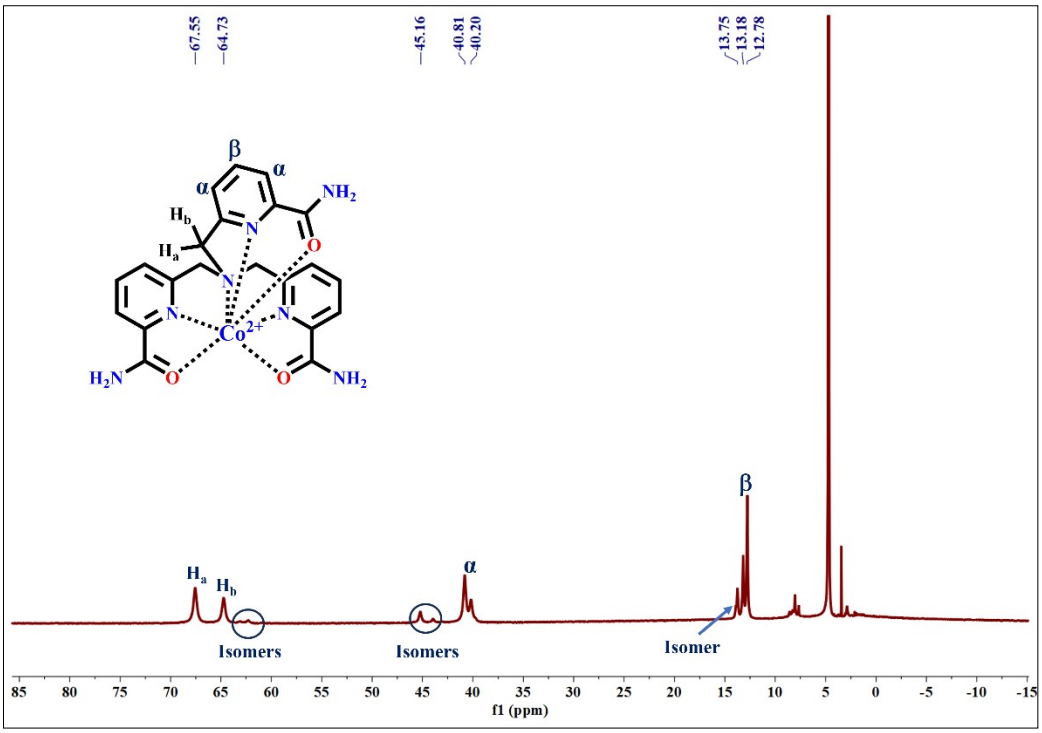

Figure S27. 400 MHz NMR spectrum of the TMTP-Co complex in D_2O with the identification of all paramagnetic protons and their corresponding isomers.

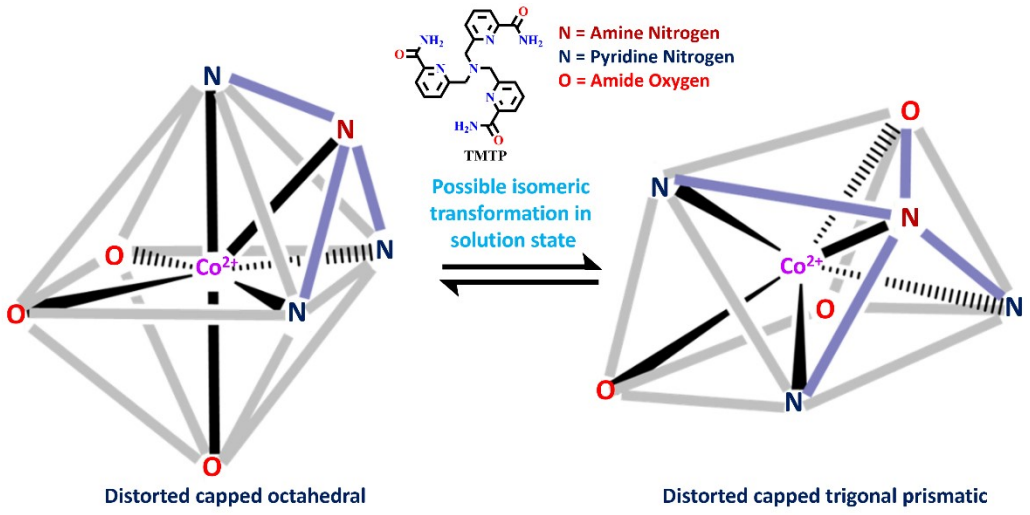

Figure S28. Possible isomers of the TMTP-Co complex in its solution state.

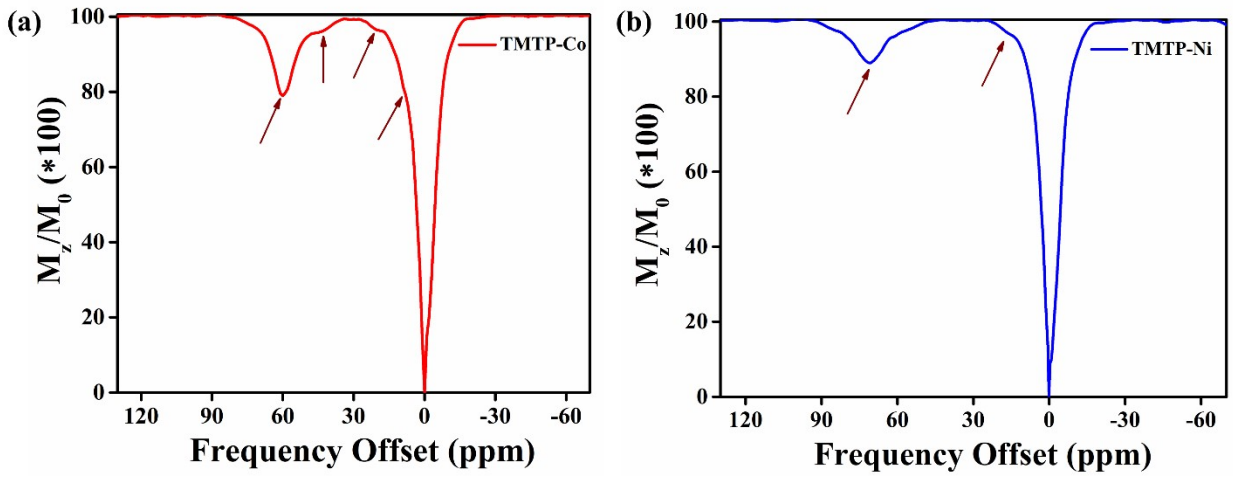

Figure S29. CEST peak positions of the amide protons in TMTP-Co and TMTP-Ni complexes.

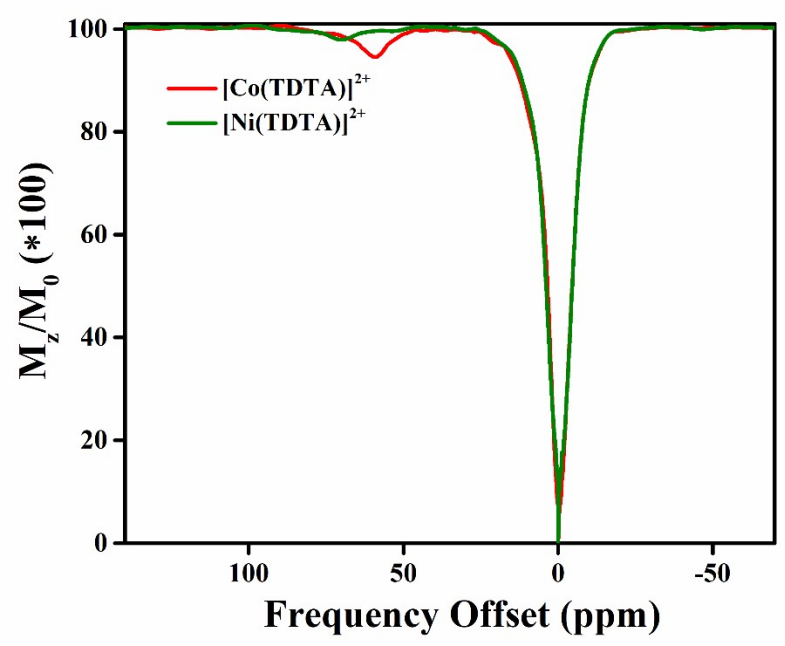

Figure S30. CEST spectra of 10 mM $[Co(TDTA)]^{2+}$ and $[Ni(TDTA)]^{2+}$ (20 mM HEPES, pH 7.4, 400 MHz) at 37 ºC with a saturation time of 4 s and saturation power of B_1 = 25 μT

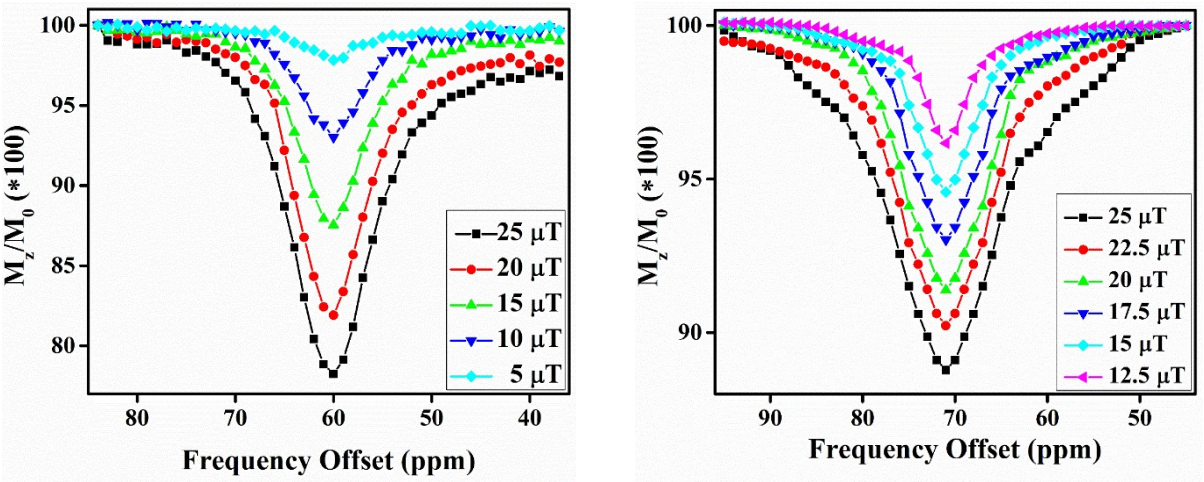

Figure S31. CEST spectra of the exchangeable proton region of 10 mM $[Co(TMTP)]^{2+}$ (left) and $[Ni(TMTP)]^{2+}$ (right) in 20 mM HEPES and 100 mM NaCl at pH 7.4 with varied pre-saturation power levels. RF pre-saturation pulse was applied for 4 s with varying saturation power of 5 µT to 25 µT for $[Co(TMTP)]^{2+}$ and 15 to 25 µT for $[Ni(TMTP)]^{2+}$.

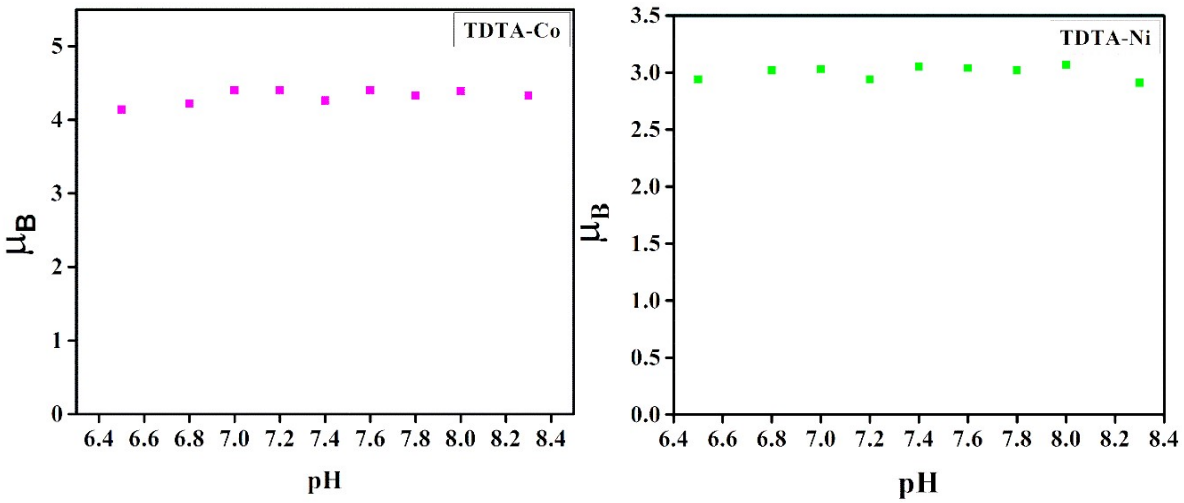

Figure S32. Solution magnetic susceptibility data for $[Co(TDTA)]^{2+}$ (left) and $[Ni(TDTA)]^{2+}$ (right) were recorded at different pH by using 3 – 5 mM complex, 20 mM HEPES, and 100 mM NaCl at 37 °C.

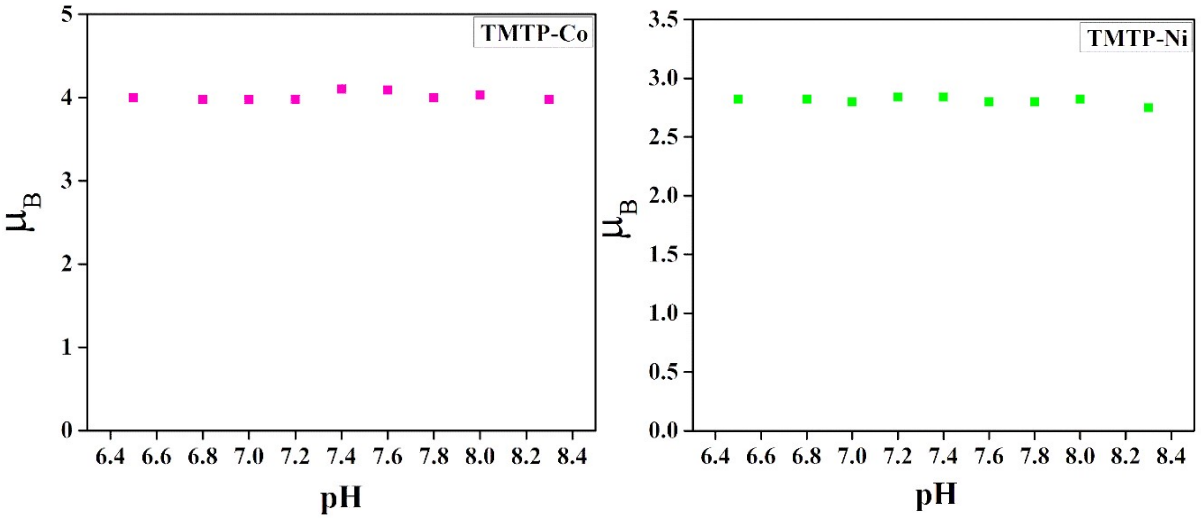

Figure S33. Solution magnetic susceptibility data for $[Co(TMTP)]^{2+}$ (left) and $[Ni(TMTP)]^{2+}$ (right) were recorded at different pH by using 3 – 5 mM complex, 20 mM HEPES, and 100 mM NaCl at 37 °C.

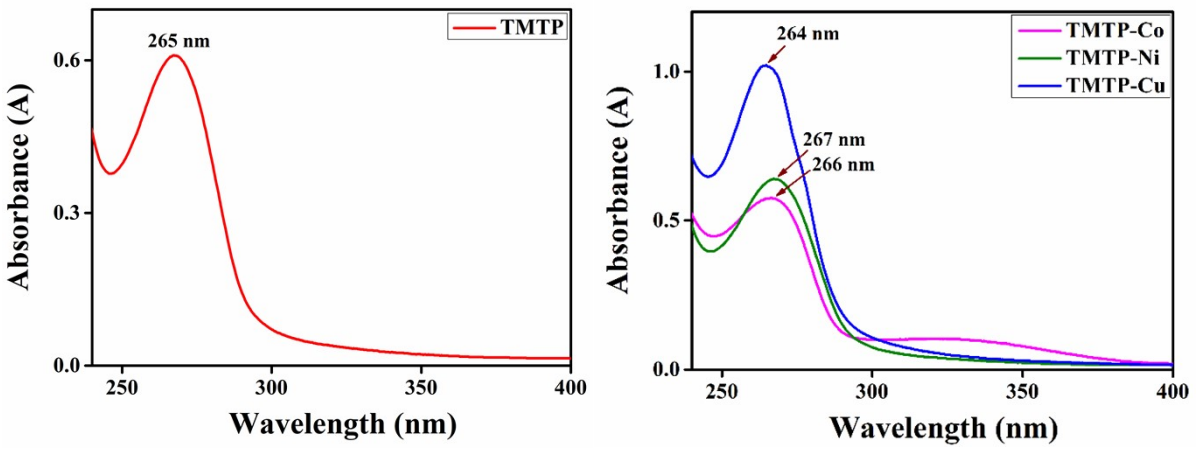

Figure S34. UV spectrum (50 µM) of the ligand TMTP (left) and its Co(II), Ni(II), and Cu(II) complexes (right), recorded in 20 mM HEPES, and 100 mM NaCl at pH 7.4.

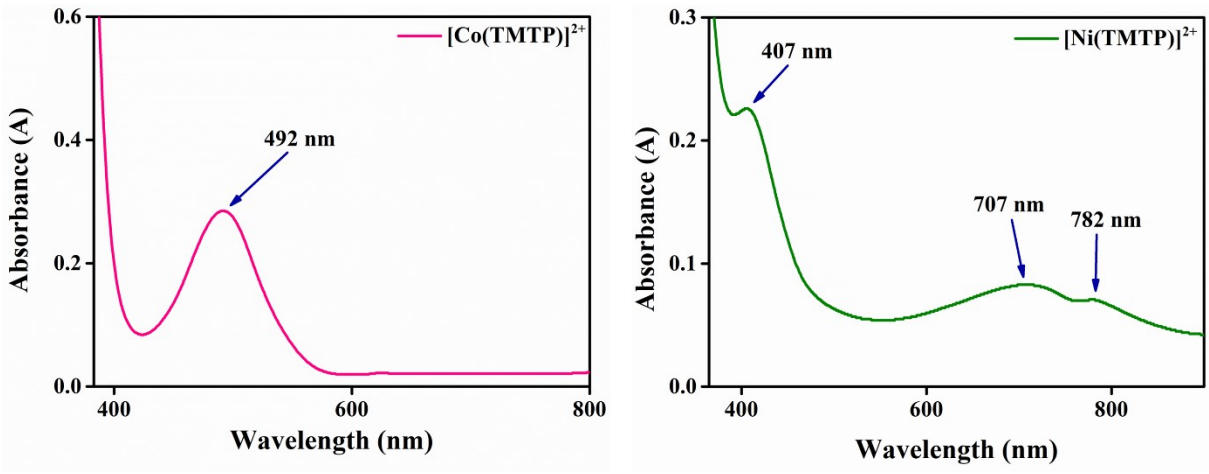

Figure S35. UV-Vis spectra of $[Co(TMTP)]^{2+}$ (left) and $[Ni(TMTP)]^{2+}$ (right) (5 mM) in 20 mM HEPES, and 100 mM NaCl at pH 7.4.

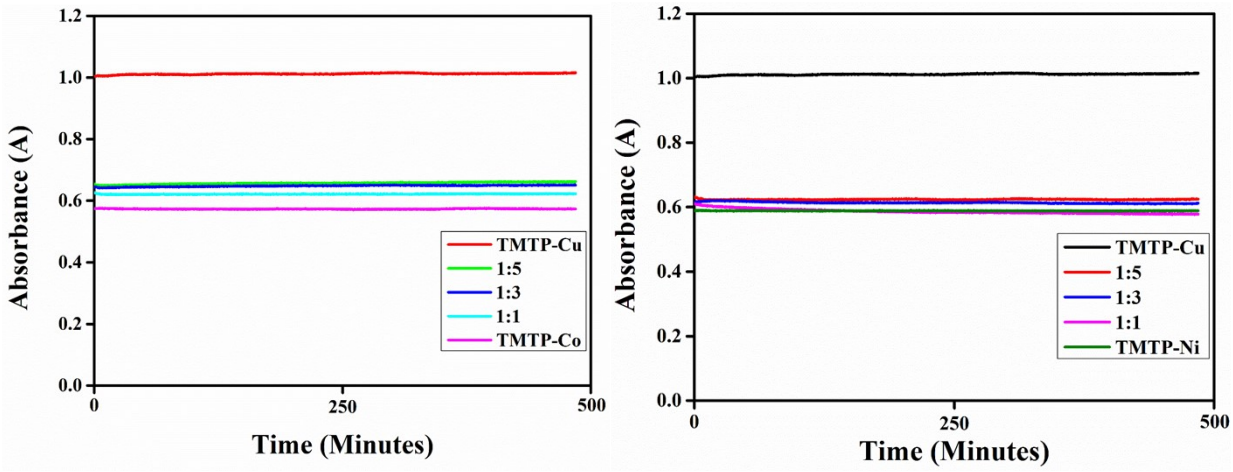

Figure S36. Metal displacement reaction of the $[Co(TMTP)]^{2+}$ and $[Ni(TMTP)]^{2+}$ complexes with competing Cu(II) ion, monitored for 8 hours at 264 nm. Samples containing 50 µM $[Co(TMTP)]^{2+}$ or $[Ni(TMTP)]^{2+}$ with 1, 2, and 5 equivalent ratios of $CuCl_2$ ions in aqueous solutions containing 20 mM HEPES and 100 mM NaCl buffered at pH 7.4. A 50 µM $[Cu(TMTP)]^{2+}$ sample is present to determine the absorbance of a 100% dissociation.

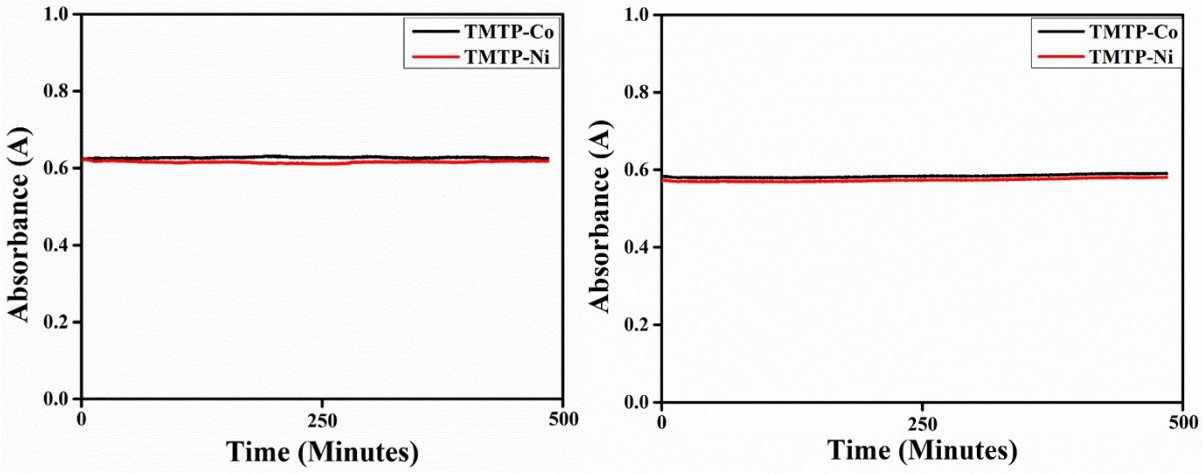

Figure S37. UV-Vis kinetic study of the complexes $[Co(TMTP)]^{2+}$ and $[Ni(TMTP)]^{2+}$ at 264 nm in acidic conditions, pH 4, (left) and in the presence of competing anions like 25 mM K_2CO_3 and 0.4 mM K_2HPO_4 (right).

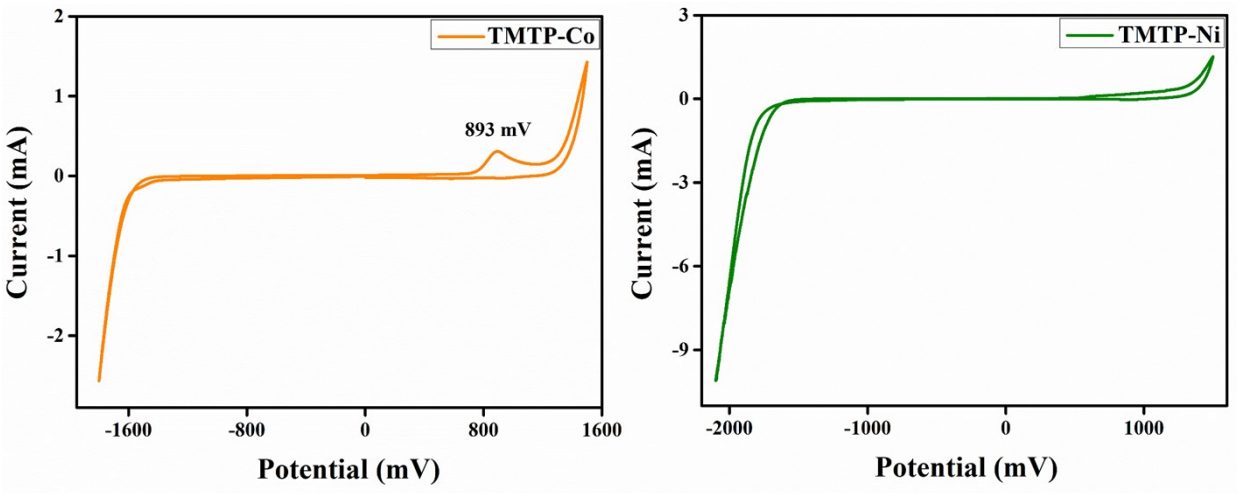

Figure S38. Cyclic voltammogram of $[Co(TMTP)]^{2+}$ (left) and $[Ni(TMTP)]^{2+}$ (right) recorded in an aqueous phase contained 1 mM complex, 20 mM HEPES, and 100 mM NaCl (pH = 7.4).

Table S1. Selected bond angles of the four complexes.

$[Co(TDTA)]\cdot 2Cl\cdot H_2O$	**$[Ni(TDTA)Cl]\cdot Cl\cdot 2H_2O$**	**$[Co(TMTP)]\cdot 2Cl$**	**$[Ni(TMTP)]\cdot 2Cl$**
Bond angles (deg)			
N(1)-Co(1)-N(3)	N(4)-Ni(1)-N(2)	N(4)-Co(1)-N(2)	O(3)-Ni(1)-O(1)
N(1)-Co(1)-N(4)	N(4)-Ni(1)-O(3)	N(4)-Co(1)-N(6)	O(3)-Ni(1)-O(2)
N(3)-Co(1)-N(4)	N(2)-Ni(1)-O(3)	N(2)-Co(1)-N(6)	O(1)-Ni(1)-O(2)
N(1)-Co(1)-O(2)	N(4)-Ni(1)-N(1)	N(4)-Co(1)-O(1)	O(3)-Ni(1)-N(3)
N(3)-Co(1)-O(2)	N(2)-Ni(1)-N(1)	N(2)-Co(1)-O(1)	O(1)-Ni(1)-N(3)
N(4)-Co(1)-O(2)	O(3)-Ni(1)-N(1)	N(6)-Co(1)-O(1)	O(2)-Ni(1)-N(3)
N(1)-Co(1)-O(1)	N(4)-Ni(1)-N(3)	N(4)-Co(1)-O(3)	O(3)-Ni(1)-N(1)
N(3)-Co(1)-O(1)	N(2)-Ni(1)-N(3)	N(2)-Co(1)-O(3)	O(1)-Ni(1)-N(1)
N(4)-Co(1)-O(1)	O(3)-Ni(1)-N(3)	N(6)-Co(1)-O(3)	O(2)-Ni(1)-N(1)
O(2)-Co(1)-O(1)	N(1)-Ni(1)-N(3)	O(1)-Co(1)-O(3)	N(3)-Ni(1)-N(1)
N(1)-Co(1)-O(3)	N(4)-Ni(1)-Cl(1)	N(4)-Co(1)-O(2)	O(3)-Ni(1)-N(4)
N(3)-Co(1)-O(3)	N(2)-Ni(1)-Cl(1)	N(2)-Co(1)-O(2)	O(1)-Ni(1)-N(4)
N(4)-Co(1)-O(3)	O(3)-Ni(1)-Cl(1)	N(6)-Co(1)-O(2)	O(2)-Ni(1)-N(4)
O(2)-Co(1)-O(3)	N(1)-Ni(1)-Cl(1)	O(1)-Co(1)-O(2)	N(3)-Ni(1)-N(4)
O(1)-Co(1)-O(3)	N(3)-Ni(1)-Cl(1)	O(3)-Co(1)-O(2)	N(1)-Ni(1)-N(4) 105.85(7)
N(1)-Co(1)-N(2)		N(4)-Co(1)-N(3)	
N(3)-Co(1)-N(2)		N(2)-Co(1)-N(3)	
N(4)-Co(1)-N(2)		N(6)-Co(1)-N(3)	
O(2)-Co(1)-N(2)		O(1)-Co(1)-N(3)	
O(1)-Co(1)-N(2)		O(3)-Co(1)-N(3)	
O(3)-Co(1)-N(2)		O(2)-Co(1)-N(3)	